

## Structure analysis of amorphous Pd<sub>75</sub>Si<sub>25</sub> alloy by electron diffraction and high-resolution electron microscopy

Mitsuhide Matsushita<sup>a,\*</sup>, Yoshihiko Hirotsu<sup>a</sup>, Tadakatsu Ohkubo<sup>a</sup>, Tetsuo Oikawa<sup>b</sup>,  
Akihiro Makino<sup>c</sup>

<sup>a</sup>The Institute of Scientific and Industrial Research, Osaka University, Ibaraki, Osaka 567, Japan

<sup>b</sup>JEOL Ltd., Akishima, 196, Japan

<sup>c</sup>Alps Elec. Co., Ltd., Higashi-Takami, Nagaoka, Niigata 940, Japan

### Abstract

A structural investigation on sputter-deposited amorphous Pd<sub>75</sub>Si<sub>25</sub> alloy thin films including the medium range order (MRO) structure has been made by means of (1) atomic pair distribution function (PDF) analysis by electron diffraction using an imaging plate (IP), (2) high-resolution electron microscopy (HREM) and (3) nano-probe electron diffraction. In the PDF profile a subpeak for the Pd–Si correlation at a distance of 0.24 nm was observed near the first main peak for the Pd–Pd correlation. MRO regions were clearly observed by HREM as lattice fringe regions with a size of 1 ~ 3 nm. Nano-probe diffraction patterns with various zone-axes beam incidences revealed that the MRO structure is hexagonal with the Pd<sub>2</sub>Si-type structure (lattice parameters:  $a = 0.715$  and  $c = 0.312$  nm, space-group:  $P\bar{6}2m$ ). In the MRO, Si atoms are thought to occupy their sites statistically to form the hexagonal structure with the Pd<sub>3</sub>Si composition. The nearest neighbor Pd–Si and Pd–Pd distances obtained from the nano-diffraction structure analysis coincided with those obtained from the PDF analysis. An examination was made on the local structure model of the present alloy.

*Keywords:* HREM; Amorphous Pd<sub>75</sub>Si<sub>25</sub>

### 1. Introduction

Atomic structures in amorphous alloys are generally understood in a statistical manner through the atomic pair distribution function (PDF) analysis mainly performed by X-ray and neutron diffraction [1,2]. On the other hand, high-resolution electron microscopy (HREM) has been applied to the observation of amorphous alloys in recent years for the visualization of local atomic structures [3–5], and medium range order (MRO) structures have been observed in various amorphous alloys [6,7].

In order to understand atomic structures in amorphous alloys comprehensively, it is now necessary to correlate averaged structural information by diffraction to local information by HREM and nano-probe electron diffraction, especially when amorphous structures

include MRO or have a nano-crystalline nature. In this study we have tried a structure analysis on sputter-deposited amorphous Pd<sub>75</sub>Si<sub>25</sub> thin films with the MRO structure. For the averaged structure, PDF analysis was made by taking advantage of the imaging plate (IP) technique which has a wide dynamic range and excellent linearity for electron intensity [8,9]. For the local structure analysis, nano-probe electron diffraction was applied to the MRO structure analysis. MRO morphologies were studied by HREM.

### 2. Experimental

Thin amorphous Pd<sub>75</sub>Si<sub>25</sub> films with thicknesses of about 6 to 10 nm were deposited on NaCl substrates in an Ar-beam sputtering device with a cryo-pump evacuation system. The substrate temperature was kept below room temperature during sputtering by cooling the substrate. An alloy disk with a composition of Pd<sub>70</sub>Si<sub>30</sub>

\* Corresponding author.

was used as the sputtering target. The compositions of the films were determined by energy dispersive X-ray spectroscopy with the help of reference samples.

Diffraction intensity in selected-area electron diffraction (SAED) was recorded and read by using a TEM-IP system (PIXsysTEM) [8]. The intensity was recorded on IP equipped in a 200 kV electron microscope (JEM-2010). The pixel size of IP was  $50 \times 50 \mu\text{m}^2$  and the intensity recorded was divided by 4096 grey levels. The intensities were digitized using a work-station computer which was followed by the PDF analysis. In order to collect only the elastic electron intensities, inelastic intensities were removed by taking advantage of electron energy-loss spectroscopy (EELS). The detail of the procedure is reported elsewhere [10]. Nano-probe electron diffraction was performed using a field-emission transmission electron microscope (FE-TEM: JEM-2010F) operating at 200 kV. In recording the diffraction patterns, both IP and electron microscopic film recording were used. In the nano-diffraction, the camera-length was corrected by using a reference nano-diffraction pattern from fine gold particles. Structural observations by HREM, and a supplemental specimen heating experiment were made in an electron microscope operating at 200 kV (JEM-2010).

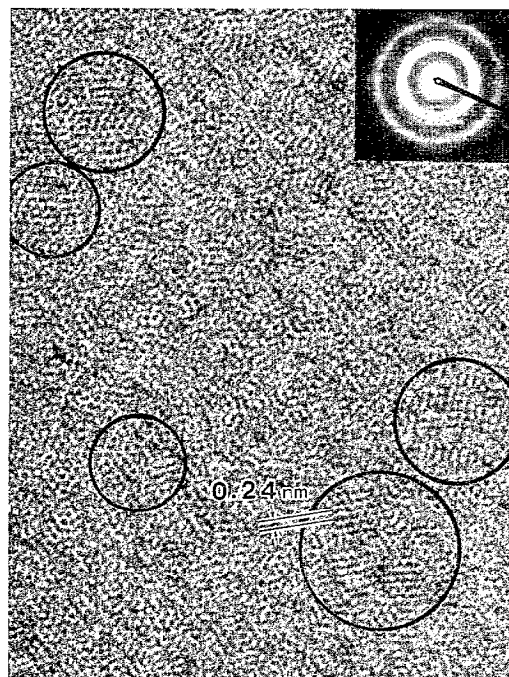


Fig. 2. HREM image of an amorphous Pd<sub>75</sub>Si<sub>25</sub> alloy thin film. MRO regions with clear cross-lattice fringes are encircled. In spite of the dense formation of the MRO regions, the halo-diffraction pattern is taken by SAED (see in the inset).

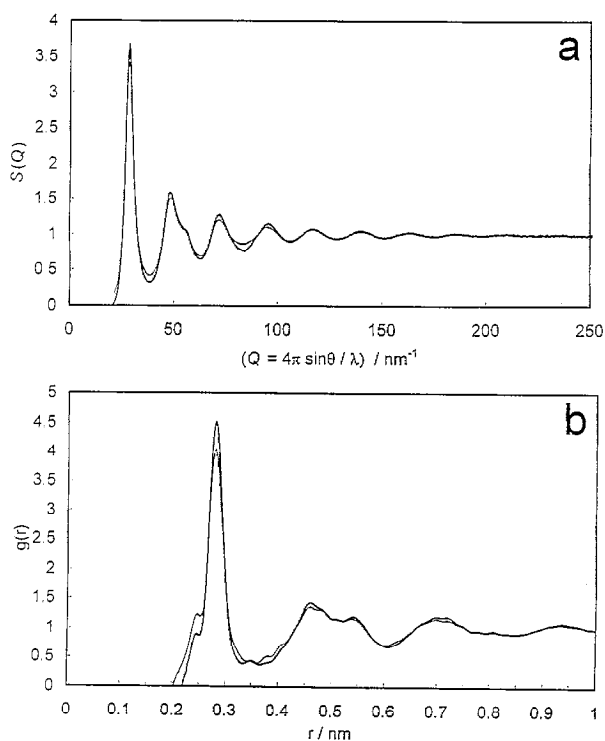


Fig. 1. (a) Structure factors of an amorphous Pd<sub>75</sub>Si<sub>25</sub> alloy thin film. Bold curve represents  $S(Q)$  with elastic scattering. Light curve,  $S(Q)$  with total scattering. (b) PDF profiles of the amorphous Pd<sub>75</sub>Si<sub>25</sub> alloy thin film obtained from  $S(Q)$  with elastic scattering (bold) and from  $S(Q)$  with total scattering (light).

### 3. Results and discussion

#### 3.1. PDF analysis by electron diffraction

Diffraction patterns by SAED were recorded on the IP with two different exposure times of 0.2 and 45 s under the same camera-length (corrected using a diffraction pattern from Au reference particles), and their intensities were normalized at a common scattering angle position, in order to measure intensities from the wide scattering angle range. Averaged intensities were obtained along the radial direction in reciprocal space up to the scattering vector  $Q = 250 \text{ nm}^{-1}$  ( $Q = 4\pi \sin \theta / \lambda$ ;  $\theta$  is the half scattering angle and  $\lambda$ , the electron wavelength). In EELS plasmon-loss peaks were clearly observed especially at the low scattering angle side. EELS profiles were recorded step-wise with respect to the scattering angle. From the ratio of the elastic intensity to the total intensity, elastic intensity was obtained at each scattering angle. The ratio approaches unity when the scattering vector becomes larger than  $Q \sim 105 \text{ nm}^{-1}$  and the ratio could not be measured because of very weak inelastic intensities.

The structure factor  $S(Q)$  for the obtained elastic electron intensities is shown in Fig. 1 (a) by the bold line, while  $S(Q)$  from intensities including the inelastic intensities is shown by the light line. It is noted that the  $S(Q)$  after the inelastic intensity correction is a little

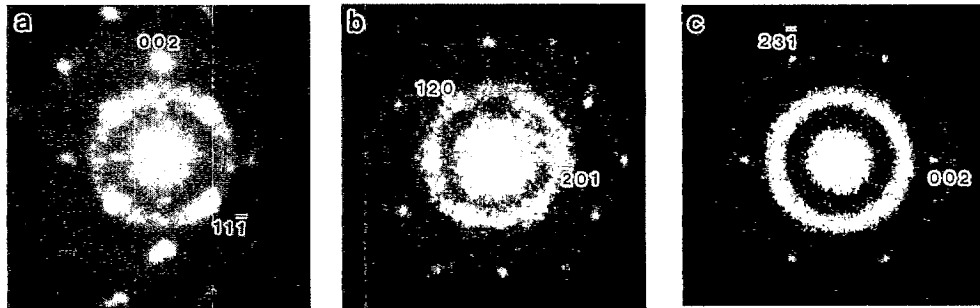


Fig. 3. Nano-diffraction patterns taken from various kinds of MRO regions with a beam size of about 1–1.5 nm. Diffraction spots are indexed according to the analyzed hexagonal structure. Beam incidences are along  $[1\bar{1}0]$  (a),  $[2\bar{1}4]$  (b) and  $[3\bar{2}0]$  (c) of the hexagonal MRO directions.

sharper. Fig. 1(b) shows the obtained PDF profile for the present  $\text{Pd}_{75}\text{Si}_{25}$  thin film specimen. Both of the profiles with (bold line) and without (light line) the inelastic intensity correction are quite similar, but a slight difference is seen especially near, and at, the first main peak. The atomic coordination numbers obtained with and without the intensity correction are 9.27 and 8.12, respectively [10]. The value with the intensity correction is closer to that obtained by neutron diffraction for an amorphous  $\text{Pd}_{78}\text{Si}_{22}$  ribbon specimen [11]. The atomic correlation peak between Pd–Si at 0.24 nm is clearly observed beside the Pd–Pd correlation peak at 0.28 nm. In Pd–Si amorphous systems the Pd–Si peak has been observed only by neutron diffraction techniques [11]. Therefore, it is demonstrated that the IP technique is quite helpful in the PDF analysis by electron diffraction.

### 3.2. HREM images

As we already found [12] in rapidly quenched ribbon specimen with a composition of  $\text{Pd}_{75}\text{Si}_{25}$ , MRO regions with a size of about 1 to 3 nm were frequently observed as localized lattice fringe images with fringe spacings of about 0.22 to 0.24 nm. Fig. 2 shows an example of the

Table 1

The observed nano-diffraction intensities ( $I_{hkl}$ ) and calculated reflection intensity ratios ( $|F_{hkl}|^2/|F_{002}|^2 \times 100$ ) for the  $\text{Pd}_2\text{Si}$ -type MRO structure. Interplanar spacings for  $(hkl)$  planes are also given

$h k l$	$d$ [nm]	$ F_{hkl} ^2/ F_{002} ^2 \times 100$	$I_{hkl}^{obs}$
1 1 0	0.358	7.40	W
0 0 1	0.312	3.44	W
1 1 1	0.235	55.04	S
$1 \bar{2} 1$	0.235	55.04	S
1 2 0	0.234	58.86	S
2 0 1	0.220	58.55	S
0 0 2	0.156	100.00	VS
2 3 0	0.142	3.43	VW
$3 \bar{2} \bar{2}$	0.130	20.43	M
2 3 1	0.129	17.65	M

HREM image from the specimen. In spite of the observation of halo-patterns in SAED typical of the amorphous structure (in the inset), MRO regions with crossed-lattice fringes were frequently observed in the HREM images. Examples of such regions are seen in the encircled areas in Fig. 2. The MRO regions with a crossed-lattice fringe angle of about 62 degrees were frequently observed in the present  $\text{Pd}_{75}\text{Si}_{25}$ . These observed crossed-fringe angles, in addition to the above mentioned lattice fringe spacings prove that the MRO structure is different from the fcc-Pd structure which is found as the MRO structure in  $\text{Pd}_{100-x}\text{Si}_x$  amorphous alloys with  $x \sim 20$  [13]. (In the case of MRO images with the fcc-Pd structure, angles of crossed-lattice fringes for two sets of  $\{1\ 1\ 1\}$  planes are always about 70 degrees even under small-angle-tilted  $\langle 1\ 0\ 1 \rangle$  zone incident conditions [13].)

### 3.3. Nano-diffraction pattern analysis

With a beam size of about 1 ~ 1.5 nm, nano-probe electron diffraction was performed. The diffraction patterns were mainly taken by selecting areas at random, but partly taken by selecting crossed-lattice fringe areas with the help of the HREM and TV system. Fig. 3 (a), (b) and (c) show examples of the obtained nano-beam diffraction patterns. In spite of the disturbance of diffuse halo background intensities, single crystal zone-axis patterns can be observed. By analysing various zone-axis patterns it was concluded that the reciprocal lattice of the MRO structure can be explained by assuming the hexagonal  $\text{Pd}_2\text{Si}$ -type structure (spacegroup;  $P\bar{6}2m$ ) [14]. The obtained lattice parameters are  $a = 0.715$  and  $c = 0.312$  nm. They could not be explained by the orthorhombic  $\text{Pd}_3\text{Si}$  structure [15], which is well known as a stable structure isomorphous with  $\text{Fe}_3\text{C}$ , nor by other palladium silicides reported:  $\text{Pd}_5\text{Si}$  [16],  $\text{PdSi}$  [17],  $\text{Pd}_4\text{Si}$  [18] and  $\text{Pd}_9\text{Si}_2$  [19]. Table 1 shows the observed nano-diffraction intensities ( $I_{hkl}$ ) and calculated reflection intensity ratios ( $|F_{hkl}|^2/|F_{002}|^2 \times 100$ ) for the  $\text{Pd}_2\text{Si}$ -type MRO structure. Observed relative

Table 2  
Crystallographic data of the Pd<sub>2</sub>Si-type MRO structure

atoms	sites				occupancy	
3Pd	3g:	$x, 0, \frac{1}{2}$	$0, x, \frac{1}{2}$	$\bar{x}, \bar{x}, \frac{1}{2}$	$x = 0.565$	1.00
3Pd	3f:	$x, 0, 0$	$0, x, 0$	$\bar{x}, \bar{x}, 0$	$x = 0.250$	1.00
2Si	2c:	$\frac{1}{3}, \frac{2}{3}, 0$	$\frac{2}{3}, \frac{1}{3}, 0$			0.85
1Si	1b:	$0, 0, \frac{1}{2}$				0.30

Space group  $P\bar{6}2m$ ;  $a = 0.715$  nm,  $c = 0.312$  nm.

intensities with respect to the standard intensity  $I_{002}$  were found to vary for every nano-diffraction pattern with a variation range of about 20 percent. This was supposed to be due to the slight off-zone-axis excitations of the nano-diffraction net patterns and also due to the multiple-scattering. Therefore, the observed intensities were classified into five ranks for convenience. The relative intensities in the table were calculated by taking the positional parameters of Pd and occupation parameters of Si as variables so that the relative intensities became closest to those of the observed intensities. The 001 intensity became negligibly small and against the observation when we took equivalent occupancies for the two Si sites or when the occupancy at 1b is larger than that at the 2c site. To this structure a composition Pd<sub>3</sub>Si was assigned. The obtained positional parameters of Pd, and the Si occupation parameters are given in Table 2. Fig. 4 shows a schematic representation of the most possible model for the MRO structure of the Pd<sub>2</sub>Si-type which is based on the intensity calculation as mentioned above. Pd atoms at 3g sites form trigonal prisms with central Si atoms at 2c sites, while Pd at 3f sites are capping atoms for the Pd(3g) prisms but also form trigonal prisms with central Si at 1b sites. From the structure determined, we can get information on the nearest neighbor atomic distances. The nearest Pd–Pd and Pd–Si distances ob-

tained are 0.27(4) and 0.23(7) nm, respectively, which are quite close to those obtained from our PDF analysis.

On the basis of coherent beam nano-diffraction theory [20] nano-diffraction patterns for the hexagonal MRO structure were calculated [21]. The calculation was made for a structure model with the central spherical MRO embedded in a dense-random packing (DRP) structure of Pd–Si atoms. The calculated diffraction patterns could explain the obtained diffraction patterns quite well. It was also found that intensities scattered from the MRO regions are easily weakened by the multiple scattering between the waves scattered from MRO and DRP regions even in the case of the structure with a total thickness of 9 nm. Based on the calculation, it was demonstrated that [001] zone-axis pattern from the hexagonal MRO easily fades away in the scattering process and intensities and arrangements of strong diffraction spots with 6-fold symmetry on the first halo-diffraction ring drastically change. This is the reason why [001] pattern from the MRO can hardly be observed by the nano-diffraction in the as-formed specimen. The 6-fold [001] diffraction pattern could be observed in the specimen annealed at 170 °C [21].

#### 3.4. Amorphous structure model and PDF calculation

On the basis of MRO structure and its morphology investigated in the present study by nano-diffraction and HREM, we can make an amorphous structure model which characterizes the present amorphous Pd<sub>75</sub>Si<sub>25</sub> alloy structure. As a trial model, a spherical MRO (hexagonal-Pd<sub>3</sub>Si structure) with a size of 2.2 nm was made and was centered in a giant cell with a size of  $3.2 \times 3.2 \times 3.2$  nm<sup>3</sup>. The central MRO was composed of about 400 Pd–Si atoms and was embedded in about 1800 DRP atoms with the Pd<sub>75</sub>Si<sub>25</sub> composition. Then the structure was relaxed by using Lennard–Jones atomic potentials for the Pd–Pd, Pd–Si and Si–Si atom pairs [22] under the periodic boundary condition. The shape of the calculated PDF roughly corresponds to that observed. It was found that the calculated PDF in this study gives a better correspondence to the observed PDF, than in our previous model in which the orthorhombic-Pd<sub>3</sub>Si MRO was embedded in DRP structure [10].

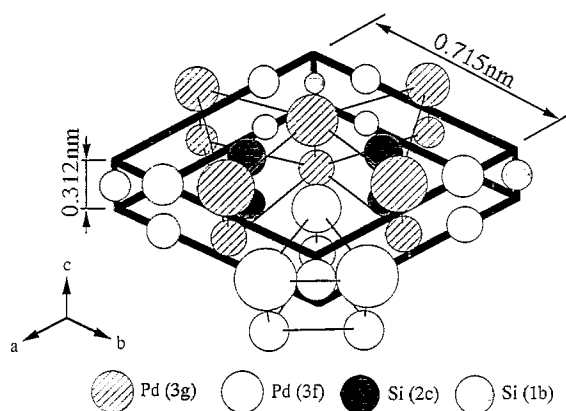


Fig. 4. Schematic representation of the hexagonal Pd<sub>3</sub>Si structure. Lattice parameters:  $a = 0.715$  nm,  $c = 0.312$  nm. Trigonal prisms formed by Pd atoms are seen.

## Acknowledgements

This work was partly supported by Grant-in-Aid for Scientific Research from the Ministry of Education, Science and Culture, Japan.

## References

- [1] S.R. Elliott, *Physics of amorphous materials*, Wiley, New York, 1990, Chap. 3.
- [2] C.N.J. Wagner, in U.Gonser (ed.), *Microscopic methods in metals, Topics in Current Physics*, Vol.40, Springer, Berlin, 1986, Chap. 5.
- [3] W.M. Stobbs and D.J. Smith, *Nature*, 281 (1979), 54.
- [4] D.J. Smith, W.M. Stobbs and W.O. Saxton, *Phil. Mag.*, B43 (1981), 907.
- [5] Y. Hirotsu and R. Akada, *Jpn. J. Appl. Phys.*, 23 (1984), L478.
- [6] Y. Hirotsu, M. Uehara and M. Ueno, *J. Appl. Phys.*, 59 (1986), 3081.
- [7] K. Anazawa, Y. Hirotsu and Y. Inoue, *Acta Metall.*, 42 (1994), 1997.
- [8] N. Mori, T. Oikawa, Y. Harada and J. Miyahara, *J. Electron Microsc.*, 39 (1990), 433.
- [9] D. Shindo, K. Hiraga, T. Oikawa and N. Mori, *J. Electron Microsc.*, 39 (1990), 449.
- [10] M. Matsushita, Y. Hirotsu, K. Anazawa, T. Ohkubo and T. Oikawa, *Mater. Trans. JIM*, 36 (1995), 822.
- [11] T. Fukunaga and K. Suzuki, *Sci. Rep. RITU*, A29 (1981), 153.
- [12] Y. Hirotsu, *Mater. Sci. Eng.*, A179/A180 (1994), 97.
- [13] Y. Hirotsu, K. Anazawa and T. Ohkubo, *Mater. Trans. JIM*, 31 (1990), 573.
- [14] A. Nylund, *Acta Chem. Scand.*, 20 (1966), 2381.
- [15] B. Aronsson, A. Nylund, *Acta Chem. Scand.*, 14 (1960), 1011.
- [16] J.A. Wysocki and P.E. Duwez, *Metall. Trans. A*, 12A (1981), 1455.
- [17] I. Engstrom, *Acta Chem. Scand.*, 24 (1970), 1466.
- [18] C. Canali, L. Silvestri and G. Celotti, *J. Appl. Phys.*, 50 (1979), 5768.
- [19] Y. Andersson, *Chem. Scr.*, 28 (1988), 125.
- [20] J.M. Zuo and J.C.H. Spence, *Phil. Mag.*, A68 (1993), 1055.
- [21] M. Matsushita, Y. Hirotsu, T. Ohkubo and T. Oikawa, *J. Electron Microsc.*, 45 (1996) 105.
- [22] J.M. Dubois, P.H. Gaskell and G. LeCaer, *Proc. R. Soc. Lond.*, A402 (1985), 323.